Simulation of nonlinear Westervelt equation for the investigation of acoustic streaming and nonlinear propagation effects

Maxim Solovchuk and Tony W. H. Sheu[a)]
Center of Advanced Study in Theoretical Sciences (CASTS), National Taiwan University, No. 1, Sec. 4, Roosevelt Road, Taipei 10617, Taiwan

Marc Thiriet
LJLL University of Paris # 6, Paris, France

(Received 20 August 2012; revised 23 May 2013; accepted 9 July 2013)

This study investigates the influence of blood flow on temperature distribution during high-intensity focused ultrasound (HIFU) ablation of liver tumors. A three-dimensional acoustic-thermal-hydrodynamic coupling model is developed to compute the temperature field in the hepatic cancerous region. The model is based on the nonlinear Westervelt equation, bioheat equations for the perfused tissue and blood flow domains. The nonlinear Navier-Stokes equations are employed to describe the flow in large blood vessels. The effect of acoustic streaming is also taken into account in the present HIFU simulation study. A simulation of the Westervelt equation requires a prohibitively large amount of computer resources. Therefore a sixth-order accurate acoustic scheme in three-point stencil was developed for effectively solving the nonlinear wave equation. Results show that focused ultrasound beam with the peak intensity 2470 W/cm^2 can induce acoustic streaming velocities up to 75 cm/s in the vessel with a diameter of 3 mm. The predicted temperature difference for the cases considered with and without acoustic streaming effect is 13.5 °C or 81% on the blood vessel wall for the vein. Tumor necrosis was studied in a region close to major vessels. The theoretical feasibility to safely necrotize the tumors close to major hepatic arteries and veins was shown.
 [http://dx.doi.org/10.1121/1.4821201]

PACS number(s): 43.80.Sh, 43.25.Nm, 43.80.Gx [SWY] Pages: 3931–3942

I. INTRODUCTION

High intensity focused ultrasound (HIFU) is a rapidly developing therapeutic method for a non-invasive ablation of benign and malignant tumors.[1,2] The main mechanism of tissue ablation is thermal coagulation. A temperature of 56 °C for 1 s heating can cause irreversible tissue damage.[3,4] Liver cancer is the second leading cause of death in Asia[5] and is now known as one of the leading causes of death in the world. The main problem in the thermal ablation therapy of a liver tumor is a heat sink due to the blood flow in large blood vessels. Convective cooling protects tumor cells from thermal destruction[6,7] and causes consequently the recurrent cancer. Special care should be taken to avoid destruction of the vessel wall by a high temperature. One clinical trial[8] showed that HIFU can safely necrotize the tumors close to major hepatic veins. Before HIFU treatment some patients had trans catheter chemoembolization. After a single session of HIFU treatment, the rate of complete necrosis was about 50%, which is not satisfactory at all. Lack of a complete response can be attributed to the large tumor size and the cooling effect in large vessels. A basic understanding of the factors that can influence altogether the tissue necrosis volume is necessary to improve thermoablative therapy and prevent recurrence.

The liver gets a blood supply from the hepatic artery and portal vein. In most of the computational studies, the liver is considered as a homogeneous tissue, and the amount of the dissipated heat is usually estimated by averaging the effect of blood perfusion over all tissues.[9–11] This approach is valid for tissues with capillaries. However, for tissues with thermally significant blood vessels (diameters larger than 0.5 mm) the biologically relevant convective cooling needs to be taken into account,[12,13] and homogenization assumption is no longer valid. Kolios *et al.*[12] and Curra *et al.*[14] studied the influence of blood vessels on the lesion size. They carried out a two-dimensional finite difference calculation in a cylindrical coordinate system. The focal point was at the center of the blood vessel. In this case a large part of the deposited ultrasound energy was carried away by convective cooling. Recently, a three-dimensional (3D) model to determine the influence of blood flow on the temperature distribution was presented.[15,16] In this case the numerical experiments can be carried out in a patient specific liver model.[15] To get velocity distribution for a real blood vessel geometry nonlinear hemodynamic equations were used. An acoustic streaming effect was taken into account. The moderate intensity regime was studied, and the model was based on the linear wave equation. In the current study, a nonlinear acoustic wave equation will be investigated.

At high intensities nonlinear wave propagation effects lead to the distortion of the wave-form. Higher harmonics are generated due to the nonlinear distortion. These higher harmonics are more readily absorbed by the tissue and enhance therefore the local heating. The two most popular

[a)]Author to whom correspondence should be addressed. Also at: Engineering Science and Ocean Engineering Department, National Taiwan University, No. 1, Sec. 4, Roosevelt Road, Taipei 10617, Taiwan. Electronic mail: twhsheu@ntu.edu.tw

nonlinear models chosen for the simulation of focused ultrasound fields are Khokhlov-Zabolotskaya-Kuznetsov (KZK) and Westervelt equations. The KZK equation is valid for directional sound beams and can be applied for transducers with aperture angles smaller than 16° to 18°.[17,18] An appropriate choice of boundary condition for the KZK equation can extend its area of applicability.[19] However for wide aperture angles it is better to use the more general Westervelt equation.[20,21] The transducer in the current study has an aperture angle of 30°. The nonlinear Westervelt equation is therefore chosen for the simulation carried out in this paper. In the moderate intensity regime, when linear theory is valid, it was shown[12,16,22] that tissue close to the blood vessel wall cannot be ablated and remains viable due to the blood flow cooling, which can cause the regeneration of a tumor. In the present paper, it will be first theoretically shown that a tumor close to the blood vessel wall can be ablated in the high-intensity regime. High focal intensity and small exposure time are two factors to ablate tumors proximal to large blood vessels. Nonlinear propagation effects can also help to ablate a tumor in this case. The presented computational model can be applied for the patient specific liver geometry.[15,23]

The propagation of ultrasound in a viscous fluid induces an additional mass flow. This effect is known as the acoustic streaming. Acoustic streaming has been observed in the cyst fluid in the breast, ovary, and testicle.[24,25] Streaming has been suggested as a diagnostic tool to differentiate cysts from solid lesions.[24] Detection of streaming can help to improve hemorrhage diagnosis. Analytical results of the earlier studies[26,27] cannot be applied to predict the acoustic streaming velocities in blood vessels during HIFU therapy.[28] Acoustic streaming can enhance blood flow cooling and strengthen the heat sink. In previous models, acoustic streaming velocity in a blood vessel during HIFU therapy was assumed to be less than blood flow velocity[29] and was neglected.[30] Recently, we showed that in the moderate-intensity regime acoustic streaming in the hepatic vein may affect the temperature distribution in a tumor.[16,31] In the artery, where the blood flow velocity is larger than that in the vein, the effect of acoustic streaming on the tissue heating was negligible. In the current study it will be shown that in the high-intensity regime acoustic streaming velocity magnitude can be 3 to 30 times larger than the velocity in a blood vessel and can be the main cooling mechanism during focused ultrasound treatment. In the current study the importance of the effects of nonlinearity, blood flow cooling, and acoustic streaming will be investigated.

II. MATHEMATICAL MODEL

A. Nonlinear acoustic equation with relaxation

An acoustic field generated by a HIFU source was modeled using the nonlinear Westervelt equation:[32,33]

$$\nabla^2 p - \frac{1}{c_0^2}\frac{\partial^2 p}{\partial t^2} + \left[\frac{\delta}{c_0^4} + \frac{2}{c_0^3}\sum_\nu \frac{c_\nu \tau_\nu}{1+\tau_\nu \frac{\partial}{\partial t}}\right]\frac{\partial^3 p}{\partial t^3} + \frac{\beta}{\rho_0 c_0^4}\frac{\partial^2 p^2}{\partial t^2} = 0. \tag{1}$$

In the above, p is the sound pressure, $\beta = 1 + B/2A$ is the coefficient of nonlinearity, and δ is diffusivity of sound resulting from viscosity and heat conduction, τ_ν is the relaxation time, and c_ν is the small signal sound speed increment for the νth relaxation process. The first two terms describe the linear lossless wave propagating at a small-signal sound speed. The third term represents the loss due to thermal conduction and fluid viscosity, and the fourth term accounts for the relaxation processes. The last term accounts for acoustic nonlinearity which may considerably affect thermal and mechanical changes within the tissue.

Following the idea proposed by Pierce[34] (p. 587), we can define the following new variable:

$$P_\nu = \frac{2}{c_0^3}\frac{c_\nu \tau_\nu}{1+\tau_\nu \frac{\partial}{\partial t}}\frac{\partial^3 p}{\partial t^3}. \tag{2}$$

This equation can be rewritten in the form as follows:

$$\left(1+\tau_\nu \frac{\partial}{\partial t}\right)P_\nu = \frac{2}{c_0^3} c_\nu \tau_\nu \frac{\partial^3 p}{\partial t^3}. \tag{3}$$

Thanks to the above two equations, Eq. (1) turns out to be identical to the coupled system of partial differential equations given below

$$\begin{aligned} &\nabla^2 p - \frac{1}{c_0^2}\frac{\partial^2 p}{\partial t^2} + \frac{\delta}{c_0^4}\frac{\partial^3 p}{\partial t^3} + \frac{\beta}{\rho_0 c_0^4}\frac{\partial^2 p^2}{\partial t^2} + \sum_\nu P_\nu = 0, \\ &\left(1+\tau_\nu \frac{\partial}{\partial t}\right)P_\nu = \frac{2}{c_0^3} c_\nu \tau_\nu \frac{\partial^3 p}{\partial t^3}. \end{aligned} \tag{4}$$

In order to investigate the importance of nonlinear effects, our calculations were performed for linear and nonlinear Westervelt equations. In the linear case, the intensity is equal to $I_L = p^2/2\rho c_0$. For the nonlinear case the total intensity is

$$I = \sum_{n=1}^{\infty} I_n, \tag{5}$$

where I_n are intensities for the respective harmonics nf_0. The ultrasound power deposition per unit volume is calculated as follows:

$$q = \sum_{n=1}^{\infty} 2\alpha(nf_0) I_n. \tag{6}$$

The absorption in tissue shown above obeys the following frequency law:

$$\alpha = \alpha_0 \left(\frac{f}{f_0}\right)^\eta, \tag{7}$$

where $\alpha_0 = 8.1$ Np/m, $\eta = 1.0$, and $f_0 = 1$ MHz.

The original Westervelt equation was derived for thermoviscous fluids. The attenuation in a thermoviscous fluid depends on the frequency squared. However, in tissues attenuation depends almost linearly on frequency. The Westervelt

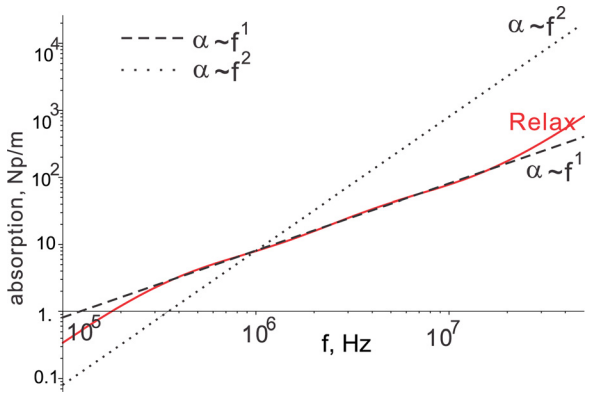

FIG. 1. (Color online) Absorption as a function of frequency for different absorption laws: Linear absorption law f^1 (dashed line), f^2 absorption (dotted line), and the fitted absorption law with two relaxation processes and thermoviscous absorption (solid line).

equation can be generalized for an arbitrary frequency dependent absorption law, if relaxation effects are taken into account. Each relaxation process has the characteristic relaxation time τ_ν and the small signal sound speed increment c_ν. Absorption coefficient at frequency ω_n has the following form:[32]

$$\alpha_n = \alpha_{\mathrm{TV}}\omega_n^2 + \frac{1}{c_0^2}\sum_\nu \frac{c_\nu \tau_\nu \omega_n^2}{1+(\omega_n\tau_\nu)^2}, \tag{8}$$

where α_{TV} denotes the thermoviscous absorption coefficient.

In the current work two relaxation processes are considered. The absorption coefficient is written in the form

$$\alpha_n = \alpha_{\mathrm{TV}}\omega_n^2 + \frac{1}{c_0^2}\frac{c_1\tau_1\omega_n^2}{1+(\omega_n\tau_1)^2} + \frac{1}{c_0^2}\frac{c_2\tau_2\omega_n^2}{1+(\omega_n\tau_2)^2}. \tag{9}$$

There are five unknown parameters α_{TV}, c_1, τ_1, c_2, and τ_2 shown in Eq. (9). These parameters were calculated by minimizing a mean square error[35] between the tissue attenuation in Eq. (7) and relaxation model (9) over the frequency band of 500 kHz to 20 MHz. These calculated parameters are $\tau_1 = 2.3369\times10^{-6}/2\pi$ s, $\tau_2 = 2.3519\times10^{-7}/2\pi$ s, $\alpha_{\mathrm{TV}} = 3.0407\times10^{-13}$ Np/m/Hz,[2] $c_1 = 5.3229$ m/s, and $c_2 = 4.3323$ m/s. The diffusivity of sound is $\delta = 2c_0^3\alpha_{\mathrm{TV}}/\omega_0^2$. In Fig. 1 the comparison between the linear absorption law and the fitted absorption law with two relaxation processes is presented. There is an excellent agreement between two relaxation laws for the frequency range of current interest.

To close the Westervelt equation, both initial and boundary conditions need to be specified. Usually the first-order non-reflecting boundary condition, which is normally used in the simulation of linearized lossless wave equation $\nabla^2 p - (1/c_0^2)(\partial^2 p/\partial t^2) = 0$, is used,

$$\frac{\partial p}{\partial n} = -\frac{1}{c}\frac{\partial p}{\partial t}. \tag{10}$$

This equation, which is valid for a plane wave of normal incidence, for the considered geometry of the problem can produce a small reflection from the boundary. To further reduce artificial reflection, a perfectly matched layer can be applied.[36] However, for the highly focused beam considered in the present study, the artificial reflection caused by Eq. (10) can be neglected. A comparison of the pressure field along the beam axis in Fig. 2(b) shows excellent agreement with the exact solution. A sinusoidal waveform was considered to be uniformly distributed over the transducer surface. The boundary condition for the source was set in a way similar to the work of Hallaj and Cleveland.[37]

The term $(\partial/\partial t)P_\nu$ in the second equation of the system (4) is approximated by the scheme with the second-order accuracy in time

$$\frac{\partial}{\partial t}P_\nu^{n+1} = \frac{1}{2\Delta t}(3P_\nu^{n+1} - 4P_\nu^n + P_\nu^{n-1}). \tag{11}$$

After some algebraic manipulation we can obtain

$$P_\nu^{n+1} = \frac{1}{1+1.5\tau_\nu/\Delta t}A\frac{\partial^3 p^{n+1}}{\partial t^3} + \frac{\tau_\nu}{2+3\tau_\nu/\Delta t}(-4P_\nu^n + P_\nu^{n-1}), \tag{12}$$

where $A = (2/c_0^3)c_\nu\tau_\nu$. P_ν^{n+1} is then substituted into the first equation of the system (4). The resulting equation which will be solved implicitly by the method is described in Sec. II D.

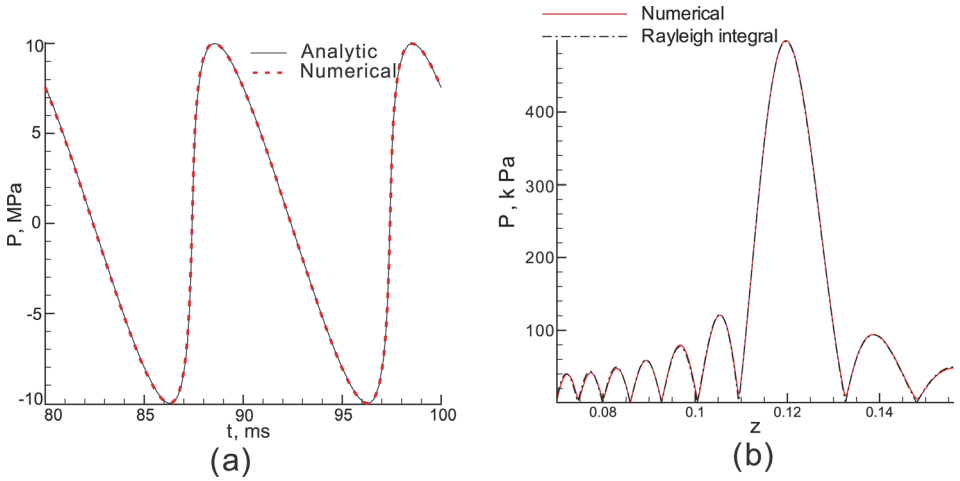

FIG. 2. (Color online) Verification of the numerical model. (a) Comparison between the numerical and analytical pressure waveform solutions at $x = 0.864\sigma$. (b) Comparison of the results predicted from the present numerical scheme for the 3D linear Westervelt equation and Rayleigh diffraction integral equation.

B. Energy equation for tissue heating

Whereas hepatic arteries and portal veins irrigate the liver parenchyma, hepatic veins drain blood out of the liver and can, thus, be considered as a heat sink. Tumor cells in the perivascular region, as a result, may escape from an externally imposed large heat, leading possibly to a local recurrence. Therefore, the mathematical model appropriate for predicting the temperature in tissues must take the heat conduction, tissue perfusion, convective blood cooling, and heat deposition due to an incident wave into account. In the simulation of thermal field the physical domain has been split into the domains for the perfused tissue and the flowing blood.

In a region free of large blood vessels, the diffusion-type Pennes bioheat equation[9] given below will be employed to model the transfer of heat in the perfused tissue region

$$\rho_t c_t \frac{\partial T}{\partial t} = k_t \nabla^2 T - w_b c_b (T - T_\infty) + q. \tag{13}$$

In the above bioheat equation proposed for modeling the time-varying temperature in the tissue domain, ρ, c, and k denote the density, specific heat, and thermal conductivity, respectively, with the subscripts t and b referring to the tissue and blood domains. The notation T_∞ is denoted as the temperature at a remote location. The variable $w_b (\equiv 0.5\,\mathrm{kg/m^3\text{-}s})$ in Eq. (13) is the perfusion rate for the tissue cooling in capillary flows. It is noted that the above bioheat equation for T is coupled with the Westervelt equation (1) for the acoustic pressure through a power deposition term q defined in Eq. (6).

In the region containing large vessels, within which the blood flow can convect heat, the biologically relevant heat source, which is q, and the heat sink, which is $-\rho_b c_b \underline{\mathbf{u}} \cdot \nabla T$, are added to the conventional diffusion-type heat equation. The resulting energy equation given below avoids a possible high recurrence stemming from the tumor cell survival next to large vessels

$$\rho_b c_b \frac{\partial T}{\partial t} = k_b \nabla^2 T - \rho_b c_b \underline{\mathbf{u}} \cdot \nabla T + q. \tag{14}$$

In the above, $\underline{\mathbf{u}}$ is the blood flow velocity. Owing to the presence of blood flow velocity vector $\underline{\mathbf{u}}$ in the energy equation, we know that a biologically sound model for conducting HIFU simulation should comprise a coupled system of acoustic-thermal-hydrodynamic nonlinear differential equations.

A thermal dose (TD) developed by Sapareto and Dewey[4] will be applied to give us a quantitative relationship between the temperature and time for the tissue heating and the extent of cell killing. In focused ultrasound surgery (generally above 50 °C), the expression for the TD can be written as

$$\mathrm{TD} = \int_{t_0}^{t_{\mathrm{final}}} R^{(T-43)} dt \approx \sum_{t_0}^{t_{\mathrm{final}}} R^{(T-43)} \Delta t, \tag{15}$$

where $R = 2$ for $T >= 43\,^\circ\mathrm{C}$, $R = 4$ for $37\,^\circ\mathrm{C} < T < 43\,^\circ\mathrm{C}$. The value of TD required for a total necrosis ranges from 25 to 240 min in biological tissues.[4,10] According to this relation, the TD resulting from heating the tissue to 43 °C for 240 min is equivalent to that achieved by heating it to 56 °C for 1 s.

C. Acoustic streaming hydrodynamic equations

Owing to the inclusion of heat sink, which is shown on the right-hand side of Eq. (14), the velocity of blood flow plus the velocity resulting from the acoustic streaming due to the applied high-intensity ultrasound must be determined. In this study we consider that the flow in large blood vessels is incompressible and laminar. The vector equation for modeling the blood flow motion, subject to the divergence free equation $\nabla \cdot \underline{\mathbf{u}} = 0$, in the presence of acoustic stresses is as follows:[38]

$$\frac{\partial \underline{\mathbf{u}}}{\partial t} + (\underline{\mathbf{u}} \cdot \nabla)\underline{\mathbf{u}} = \frac{\mu}{\rho}\nabla^2 \underline{\mathbf{u}} - \frac{1}{\rho}\nabla \mathbf{P} + \frac{1}{\rho}\underline{\mathbf{F}}. \tag{16}$$

In the above, $\mathbf{P}$ is the static pressure, μ (=0.0035 kg/m s) is the shear viscosity of blood flow, and ρ is the blood density. In Eq. (16), the force vector $\underline{\mathbf{F}}$ acting on the blood fluid due to ultrasound is assumed to act along the acoustic axis $\underline{\mathbf{n}}$. The resulting nonzero component in $\underline{\mathbf{F}}$ takes the following form:[27]

$$\underline{\mathbf{F}} \cdot \underline{\mathbf{n}} = -\frac{1}{c_0}\nabla \vec{I} = \frac{q}{c_0}. \tag{17}$$

D. Three-point sixth-order accurate scheme for the Westervelt equation

In our previous studies the linear Westervelt equation was investigated.[13,15,16] For the linear Westervelt equation the solution can be obtained in an integral form (diffraction integral).[39] In the current work the nonlinear Westervelt equation will be solved using the implicit finite-difference time domain method. To reduce computational costs a highly accurate scheme for the Westervelt equation in a grid stencil involving only three points was developed. Discretization of the Westervelt equation (1) is started with the approximation of temporal derivatives. Temporal derivatives were approximated by second-order accurate schemes as follows:

$$\left.\frac{\partial^2 p}{\partial t^2}\right|^{n+1} = \frac{2p^{n+1} - 5p^n + 4p^{n-1} - p^{n-2}}{(\Delta t)^2}, \tag{18}$$

$$\left.\frac{\partial^3 p}{\partial t^3}\right|^{n+1} = \frac{6p^{n+1} - 23p^n + 34p^{n-1} - 24p^{n-2} + 8p^{n-3} - p^{n-4}}{2(\Delta t)^3}. \tag{19}$$

The nonlinear term $\partial^2 p^2/\partial t^2|^{n+1}$ is linearized using the second-order accurate relation

$$\begin{aligned}\left.\frac{\partial^2 p^2}{\partial t^2}\right|^{n+1} &= \left.\frac{\partial}{\partial t}\left(\frac{\partial p^2}{\partial t}\right)\right|^{n+1} \\ &= 2\frac{\partial}{\partial t}\left(p^n \left.\frac{\partial p}{\partial t}\right|^{n+1} + p^{n+1}\left.\frac{\partial p}{\partial t}\right|^{n} - p^n \left.\frac{\partial p}{\partial t}\right|^{n}\right) \\ &= 2(2p_t^n p_t^{n+1} + p^n p_{tt}^{n+1} + p^{n+1} p_{tt}^n - (p_t^n)^2 - p^n p_{tt}^n).\end{aligned} \tag{20}$$

The above Eqs. (18)–(20) are then substituted into Eq. (1) to yield the following inhomogeneous Helmholtz equation:

$$u_{xx} - ku = f(x). \tag{21}$$

High-order Helmholtz schemes can be constructed by introducing more finite-difference stencil points. The improved prediction accuracy will be, however, at the cost of an increasingly expensive matrix calculation. To retain the prediction accuracy at a lower computational cost, we are motivated to develop a scheme that can give us the accuracy order of sixth in a grid stencil involving only three points. To achieve the above goal, we define first the spatial derivatives $u^{(2)} \equiv u_{xx}, u^{(4)} \equiv u_{xxxx}$, and $u^{(6)}$ at a nodal point j as follows:

$$u^{(2)}|_j = s_j, \quad u^{(4)}|_j = t_j, \quad u^{(6)}|_j = w_j. \tag{22}$$

Development of the compact difference scheme at x_j is to relate t, s, and w with u as follows:

$$h^6\delta_0 w_j + h^4\gamma_0 t_j + h^2\beta_0 s_j = \alpha_1 u_{j+1} + \alpha_0 u_j + \alpha_{-1} u_{j-1}. \tag{23}$$

Substituting the Taylor-series expansion into Eq. (23) and conducting then a term-by-term comparison of the derivatives, the introduced free parameters can be determined as $\alpha_1 = \alpha_{-1} = -1, \alpha_0 = 2, \beta_0 = -1, \gamma_0 = -1/12$ and $\delta_0 = -1/360$.

Since $s_j = k_j u_j + f_j$, the following two expressions for $t_j = (k_j^2 u_j + 2k_{x,j}u_{x,j} + k_{xx,j}u_j + k_j f_j + f_{xx,j})$ and $w_j = (k_j^3 u_j + 7k_j u_j k_{xx,j} + 6k_j u_{x,j}k_{x,j} + 4k_{x,j}^2 u_j + 6k_{xx,j}f_j + 4k_{xxx,j}u_{x,j} + k_{xxxx,j}u_j + 4k_{x,j}f_{x,j} + k_j f_{xx,j} + f_{xxxx,j})$ resulted. Equation (23) can then be rewritten as

$$\begin{aligned}&\alpha_1 u_{j+1} + \alpha_1 u_{j-1} + [\alpha_0 - \beta_0 h^2 k_j - \gamma_0 h^4 (k_j^2 + k_{xx,j}) - \delta_0 h^6 (k_j^3 + 7k_j k_{xx,j} + 4k_{x,j}^2 + k_{xxxx,j})]u_j \\ &\quad = h^2\beta_0 f_j + h^4\gamma_0(2k_{x,j}u_{x,j} + k_j f_j + f_{xx,j}) + h^6\delta_0(k^2 f_j + k f_{xx,j} + f_{xxxx,j}) + h^6\delta_0(6k_j u_{x,j}k_{x,j} + 6k_{xx,j}f_j + 4k_{xxx,j}u_{x,j} + 4k_{x,j}f_{x,j}).\end{aligned} \tag{24}$$

It follows that

$$\begin{aligned}&\left[1 - \left(\frac{1}{2h} - \frac{k_{j+1}h}{12}\right)\left(\frac{1}{360}h^6(4k_{xxx,j} + 6k_j k_{x,j}) + \frac{1}{6}h^4 k_{x,j}\right)\right]u_{j+1} \\ &\quad - \left[2 + h^2 k_j + \frac{1}{12}h^4(k_j^2 + k_{xx,j}) + \frac{1}{360}h^6(k_j^3 + 4k_{x,j}^2 + 7k_j k_{xx,j} + k_{xxxx,j})\right]u_j \\ &\quad + \left[1 + \left(\frac{1}{2h} - \frac{k_{j-1}h}{12}\right)\left(\frac{1}{360}h^6(4k_{xxx,j} + 6k_j k_{x,j}) + \frac{h^4 k_{x,j}}{6}\right)\right]u_{j-1} \\ &\quad = \left[h^2 + \frac{k_j h^4}{12} + \frac{1}{360}h^6(k_j^2 + 6k_{xx,j})\right]f_j + \frac{1}{90}h^6 k_{x,j}f_{x,j} + \left(\frac{1}{360}h^6 k_j + \frac{1}{12}h^4\right)f_{xx,j} \\ &\quad + \frac{1}{360}h^6 f_{xxxx,j} + \left[\frac{1}{6}h^4 k_{x,j} + \frac{1}{360}h^6(6k_j k_{x,j} + 4k_{xxx,j})\right].\left[-\frac{h}{12}(f_{j+1} - f_{j-1})\right].\end{aligned} \tag{25}$$

The corresponding modified equation for Eq. (21) using the currently proposed compact difference scheme can be derived as follows after performing some algebraic manipulation:

$$\begin{aligned}u_{xx} - ku = f + \left(\frac{h^6}{20160}\right)u^{(8)} + \left(\frac{h^8}{1814400}\right)u^{(10)} \\ + \cdots + \mathrm{HOT},\end{aligned} \tag{26}$$

where HOT denotes higher order terms. The above modified equation analysis sheds light that the Helmholtz scheme developed within the three-point stencil framework can yield a spatial accuracy of sixth-order. An axisymmetric sound beam was considered. The Westervelt equation was solved in a cylindrical coordinate system in conjunction with the alternating direction implicit solution algorithm.[40] The focal point and acoustic axis were located outside of the vessel, and the acoustic field was assumed to be the same as that in the absence of the vessel.[22] This will introduce an error. Using an axisymmetric code we estimated that the error in the heating term is less than 5% for the current geometry of the problem (Fig. 3). Absorption properties of liver and blood were different in the calculations of intensity and power deposition terms. In blood it was assumed that absorption depends on frequency squared. When the focal point is located at the center of the blood vessel [Fig. 4(b)], propagation of ultrasound in blood was taken into account.

Accuracy of the numerical solutions was examined by comparing them with the known analytical and numerical solutions of other authors. For a one-dimensional plane nonlinear wave propagation problem, an analytical solution is available.[32,41] The Fubini solution is valid up to the shock formation distance $\sigma = c_0^3\rho_0/(\beta p_0\omega_0)$ in a lossless medium. The comparison of numerical and analytical solutions for the one-dimensional plane wave is presented in Fig. 2(a). For

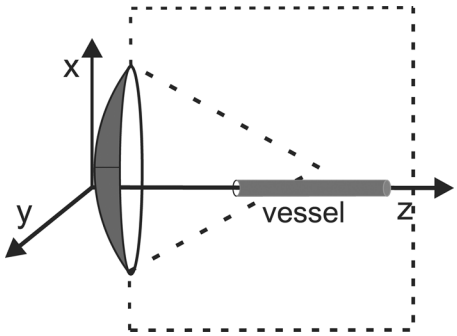

FIG. 3. Schematic of the physical model. The blood vessel is parallel to the acoustics axis. The space bounded by the dashed line and the transducer is the domain for conducting the acoustic wave simulation.

the 3D problem the results predicted with the numerical scheme for the Westervelt equation were compared with the result obtained from the Rayleigh diffraction integral equation for the linear acoustic field in Fig. 2(b).[39] We can see an excellent agreement between the numerical and analytical solutions for the pressure along the beam axis. In Fig. 5 the currently predicted results for the peak positive P_+ and negative P_- pressures at the focal point are compared quite well with the experimental data.[42]

III. RESULTS AND DISCUSSION

A. Description of the problem

The single element HIFU transducer used in this study is spherically focused with an aperture of 12 cm and a focal length of 12 cm. The parameters used in the current simulation are listed in Table I.[43]

In this study, the ultrasound of 1.0 MHz insonation is incident from a location that is exterior of the liver tumor. The acoustic propagation was assumed to be entirely in the liver. The initial temperature is equal to 37 °C. The vessel diameter is 3 mm. The fully developed velocity profile is applied at the inlet of the blood vessel, while zero gradient

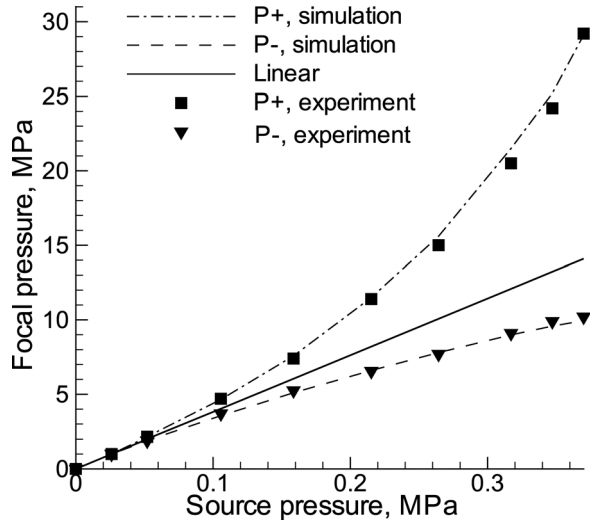

FIG. 5. The currently predicted results for the peak positive P_+ and negative P_- pressures at the focal point are compared with the experimental data (Ref. 42).

velocity boundary condition on the outlet plane. The blood vessel schematic in Fig. 3 is parallel to the acoustic axis. For parallel blood vessel orientation the effect of blood flow is maximal, therefore only this vessel orientation is considered in the present study. The computational model used in the current paper can be applied for a patient specific liver geometry geometry.[13,15,23] The inlet average velocity $u = 0.13$ m/s corresponds to the velocity in an artery. The distance between the focal point located at (0.002; 0; 0.12) and the blood vessel wall (the gap) is 0.5 mm.

Numerical implementation of the mathematical model presented in Sec. II will be described below. First the acoustic pressure was calculated. The acoustic pressure was calculated using finite difference time domain code presented in Sec. II D. Afterward ultrasound power deposition in Eq. (6) and acoustic streaming force in Eq. (17) were determined and stored. Blood flow velocity was computed from

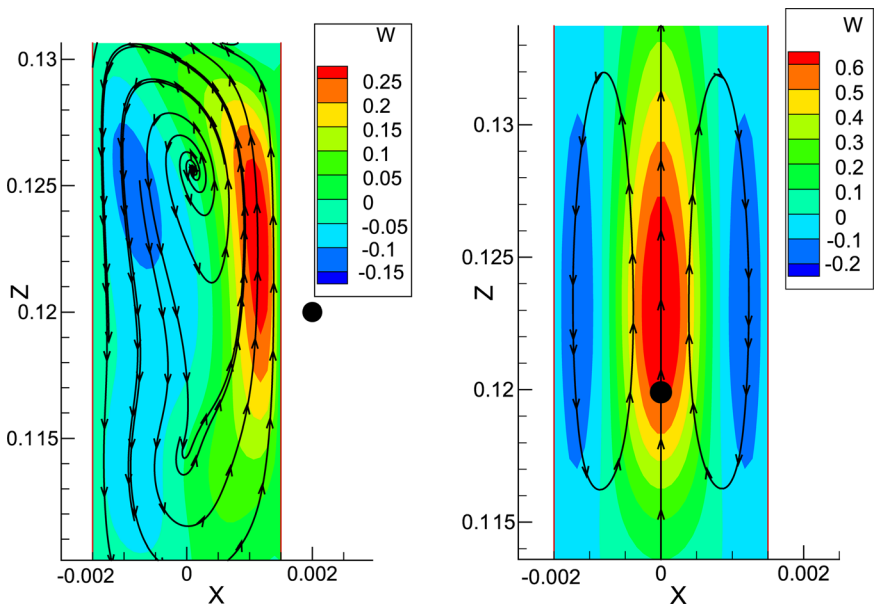

FIG. 4. (Color online) The simulated streaming profile at the cutting plane $y = 0$ without the externally applied flow (initial velocity = 0), $P_L = 8.5$ Mpa, circle denotes the focal point. (a) Focal point (•) is at a distance 0.5 mm from the vessel wall, at $x = 0.002$ m and $z = 0.12$ m; (b) focal point (•) is in the center of the blood vessel, at $x = 0$ and $z = 0.12$ m.

TABLE I. Acoustic and thermal properties for the liver tissue and blood.

Tissue	c_0 (m/s)	ρ (kg/m^3)	c (J/kgK)	k (W/mK)	α (Np/m)
Liver	1540	1055	3600	0.512	8.1
Blood	1540	1060	3770	0.53	1.5

Eq. (16) at every time step with the acoustic streaming effect being taken into account and then substituted to the bioheat Eq. (14). We have our in-house developed finite element code for solving the nonlinear hemodynamic equations.[44–46] But for convenience the commercially available CFDRC (CFDRC Research, Huntsville, AL) software was used for the 3D geometry. With known blood flow velocities and power deposition terms, temperatures in blood flow domain and in the liver were calculated using the CFDRC software in three-dimensions. A detailed description of the solution procedures can be found in our previous articles.[13,15] The 3D computational model employed in this study for the prediction of acoustic streaming field was validated by comparing the results with those of Kamakura *et al.*[38] The present computational model was also validated by comparing our simulated results for the temperature field,[16] with and without flow, with the experimental results of Huang *et al.*[47]

B. The effect of nonlinearity

The effect of acoustic nonlinearity distorts ultrasound waves and generates higher harmonics. The appearance of higher harmonics affects the amount of the absorbed energy. Previous investigations of nonlinear propagation effects for focused ultrasound transducers of high focusing gain showed that nonlinear effects are important only in a small focal area.[48] Due to the thermal diffusion the difference between the predicted lesions for the linear and nonlinear theories was negligible.[48] In Ref. 11 the HIFU transducer operating at peak intensities up to 25 000 W/cm^2 was used to heat protein phantom and liver samples. At such extremely large intensities shock waves were measured. The calculated temperature rise to 100 °C agreed well with the measured time to initiate boiling for the focal positive pressures up to 70 MPa. At such a high pressure value cavitation activity becomes very important.[49] In the present study the acoustic intensities below the shock wave formation threshold will be considered.

In Fig. 6 the predicted linear and nonlinear pressures, intensities, and power depositions as functions of the axial z and radial distances r are presented. In the simulations the ultrasound beam propagates entirely in tissue. The peak positive and negative pressures are $P_+ = 14.3$ MPa and $P_- = 6.4$ MPa, correspondingly. The linear theory predicts

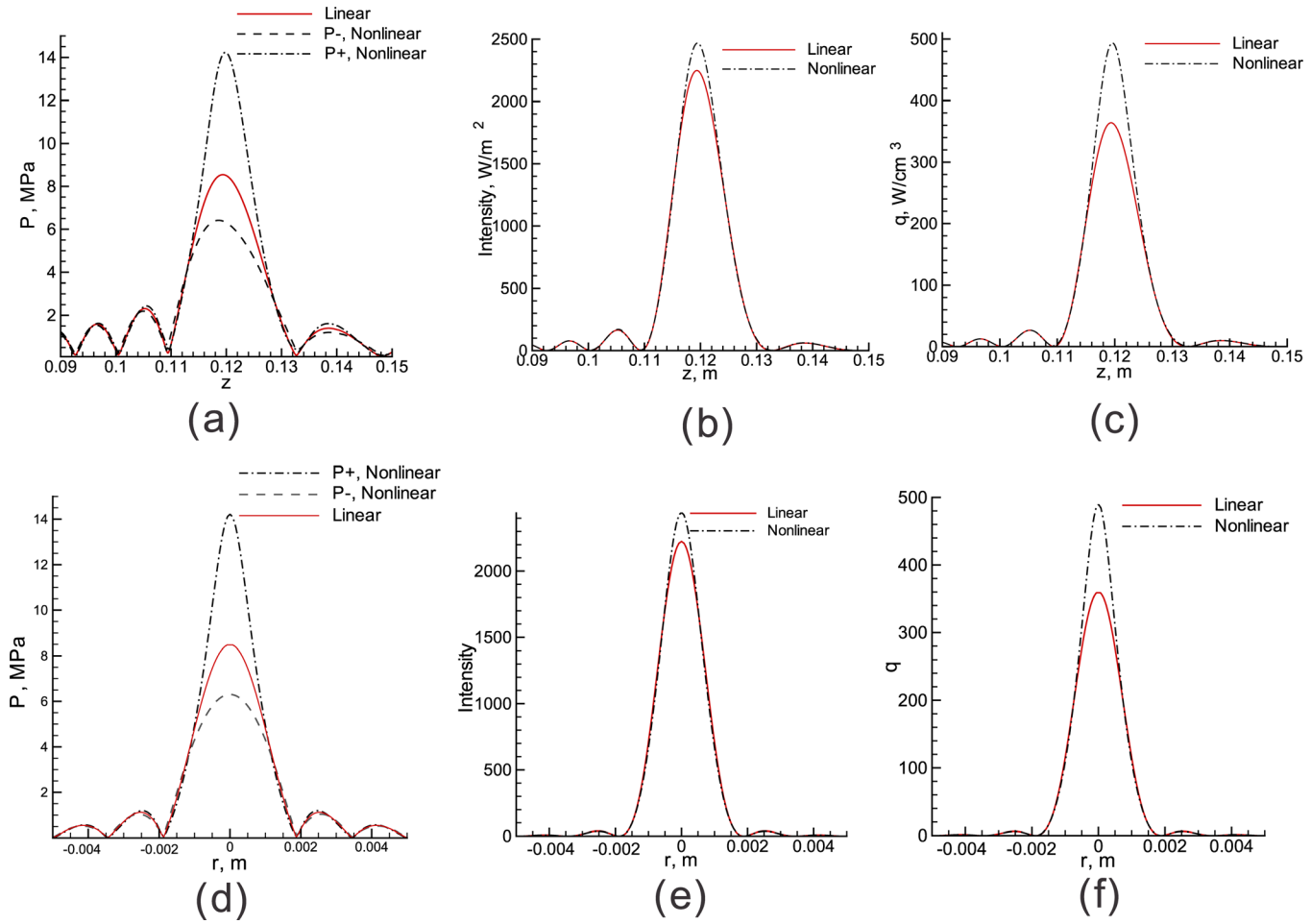

FIG. 6. (Color online) The predicted linear and nonlinear pressures [(a) and (d)], intensities [(b) and (e)], and power depositions [(c) and (f)] as functions of the axial z and radial r distances (in the focal plane).

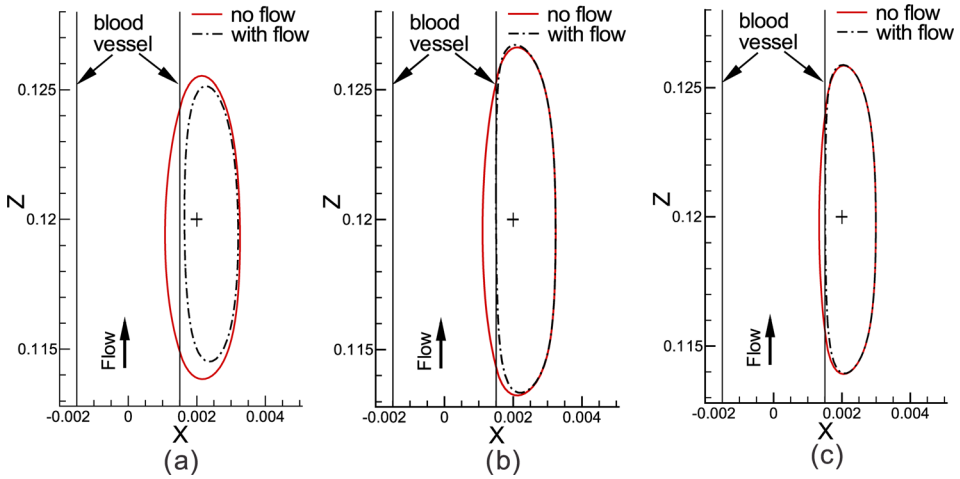

FIG. 7. (Color online) The predicted lesion shapes for the cases with and without flow at different focal intensities, cross (+) denotes the focal point, velocity = 0.13 m/s. (a) Sonication time $t = 8$ s, $P_L = 3.3$ MPa, $I_L = 340$ W/cm^2; (b) $t = 1.8$ s, $P_L = 6.37$ MPa, $I_L = 1260$ W/cm^2; (c) $t = 0.6$ s, $P_L = 8.5$ MPa, $I_L = 2240$ W/cm^2.

focal pressure $P_L = 8.5$ MPa. The linear focal intensity is $I_L = P^2/2\rho c = 2240$ W/cm^2. In Fig. 6 the peak power deposition increased 37% from the linear to nonlinear waveform. Nonlinear effects are important only in a small region of the focal area. In the following study the nonlinear Westervelt equation will be used; linear values of pressure P_L and intensity I_L will be given as a reference values (for example, in Fig. 7). Nonlinear simulation results shown in Fig. 8 indicate the peak temperature 102 °C for the exposure time of 0.7 s, while the linear theory predicts only 90 °C. These simulated results show that nonlinear propagation effects enhance heating in the focal zone and lead to boiling in tissues (temperature above 100 °C). Vapor/gas bubbles, produced in the focal zone, can reflect and scatter the ultrasound beam, thereby complicating the situation. The echogenic region in the focal area appears and the lesion starts to grow toward the transducer, thereby producing a tadpole shape.[10,50,51] It was found that before boiling the lesion grew almost symmetrically about the focus[10,50,51] and the lesion shape could be well predicted. In the following study the heating time and ultrasound power are chosen so that the maximum temperature is below 100 °C.

The predicted temperatures on the blood vessel wall (0.0015; 0; 0.12) are 55 °C and 57.4 °C for the respective linear and nonlinear Westervelt equations. The temperature 56 °C for 1 s heating can be considered as an estimated threshold value for tissues to necrose.[16] Nonlinear effects, as a result, help to ablate tumors close to large blood vessels. We can see that a tumor close to the blood vessel wall can be ablated. Inside the blood vessel there is a very fast temperature decrease due to blood flow cooling and blood temperature is below the coagulation necrosis threshold, so HIFU should not affect blood cells.[52] In the open surgery devices such as ligasure or harmonic scalpel are used to stop bleeding by heating the ruptured part of the vessel for temperatures above 60 °C.[53] Therefore we assume that if the blood vessel wall is damaged by a high temperature during HIFU treatment, bleeding should not occur (high temperature should stop bleeding). However, additional experiments and theoretical studies are necessary in order to investigate the feasibility and safety of the HIFU treatment of tumors close to the blood vessel wall.

C. The effect of acoustic streaming

Acoustic streaming is considered as a second-order physical effect in the HIFU therapy and is usually neglected. To investigate the importance of the acoustic streaming effect during thermal therapy, the hydrodynamic Eq. (16) with the acoustic source given in Eq. (17) was calculated. In Fig. 4 the z velocity component at the cutting planes $y = 0$ and streamlines are presented for two focal point locations: at a distance 0.5 mm from the vessel wall and in the center of the blood vessel. The initial velocity is equal to zero, the

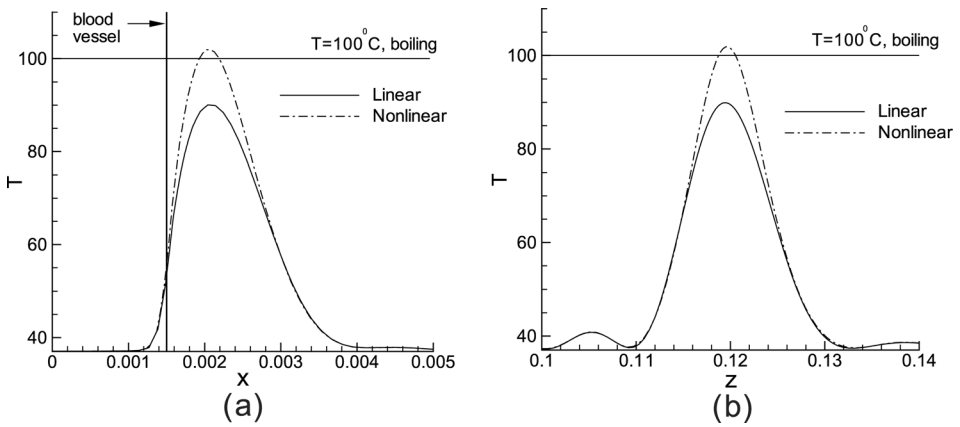

FIG. 8. The predicted temperature distributions along x (a) and z (b) directions at $t = 0.7$ s for the cases of solving linear and nonlinear Westervelt equations. The focal point is at a distance 0.5 mm from the vessel wall, at $x = 0.002$ m and $z = 0.12$ m.

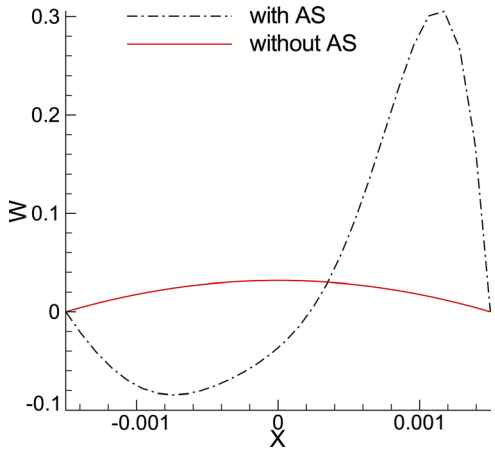

FIG. 9. (Color online) The simulated velocity profiles w (velocity in z direction) at $z = 0.123$ m for the cases with and without acoustic streaming (AS). Focal point is at a distance 0.5 mm from the vessel wall, at $x = 0.002$ m and $z = 0.12$ m, inlet average velocity is 0.016 m/s (vein).

diameter of blood vessel is $d = 3$ mm, and the gap (the distance between the focal point and the vessel wall) is 0.5 mm. Acoustic streaming velocity is induced by the absorbed ultrasound energy. The mass flow through any cross section is equal to zero due to the incompressibility of the fluid. Focused ultrasound can induce acoustic streaming velocities up to 0.31 m/s [Fig. 4(a)]. When the focal point is at the center of the blood vessel, the magnitude of acoustic streaming velocity is 0.75 m/s [Fig. 4(b)]. In Fig. 4(b) we have the axially flowing blood in the center of the blood vessel and the reverse flow near the boundary region. The total mass flow through any cross section is equal to zero. The point with the maximum velocity is located in the post-focal region owing to the mass flowing out of the focal region. The blood flow velocities vary from 0.016 m/s (corresponding to the velocity in vein) and 0.13 m/s (artery) for $d = 3$ mm. Acoustic streaming velocity magnitude is 3 to 30 times larger than the blood vessel velocity. The simulation results show that the difference between the linear and nonlinear acoustic streaming profiles is small for gaps larger than 0.5 mm. The peak velocity increases with the increasing blood vessel diameter.[13] For the diameter of blood vessel $d = 6$ mm, the magnitude of acoustic streaming velocity is 0.94 m/s, when the focal point is at the center of the blood vessel. An increase of focal intensity will cause an increase of acoustic streaming velocity magnitude and correspondingly represents an additional heat sink. It will also increase heat deposition. Nonlinear propagation effects become more pronounced for higher intensities and give an extra heat source. The combined effect of acoustic streaming, blood flow cooling, and nonlinear propagation effects will be presented in Fig. 7 for different acoustic powers.

There is a very large velocity gradient near the blood vessel wall (Fig. 4) provided that the acoustic streaming effect is taken into account. This will increase blood flow cooling and decrease temperature rise. Due to the no-slip condition on the boundary the velocity is zero on the blood vessel wall. The largest velocity gradient is near the vessel wall. The large shear stresses due to the high velocity gradient near the boundaries may cause damage of the vessel wall cells. Histological studies of mammalian tissues after irradiation with 1 MHz (Ref. 54) and 3 MHz ultrasound[55–57] showed that the walls of the blood vessels were often damaged. Collected membrane fragments were found inside the blood vessel.[56] This type of damage was thought to be a result from the generation of high shear stress associated with the acoustic streaming. In Fig. 9 the simulated velocity profiles w in a vein are presented for the cases with and without acoustic streaming. The predicted velocity gradients on the blood vessel wall for the cases with and without acoustic streaming effect differ by about 40 times. So the present study can confirm the early proposed hypothesis.

In Fig. 10 the predicted temperature distributions on the blood vessel wall are presented for a 0.6 s sonication for the cases with and without inclusion of acoustic streaming. The inlet average velocities are $u = 0.13$ m/s (artery) and $u = 0.016$ m/s (vein). At $t = 0.6$ s the temperature rise is 25 °C without the acoustic streaming (AS) effect and 16.2 °C with the AS effect. This means that the temperature rise was reduced by 54% due to the acoustic streaming effect. For smaller blood velocities (in vein $u = 0.016$ m/s) the effect of acoustic streaming becomes more pronounced (13.5 °C or 81% difference). For the case with a smaller distance between the blood vessel wall and focal point, the effect of acoustic streaming will be more important.

The predicted lesion for different focal intensities and sonication times are presented in Figs. 7(b) and 7(c). Peak temperatures below 100 °C are considered. In the moderate intensity regime [Fig. 7(a)], when the linear theory is valid,

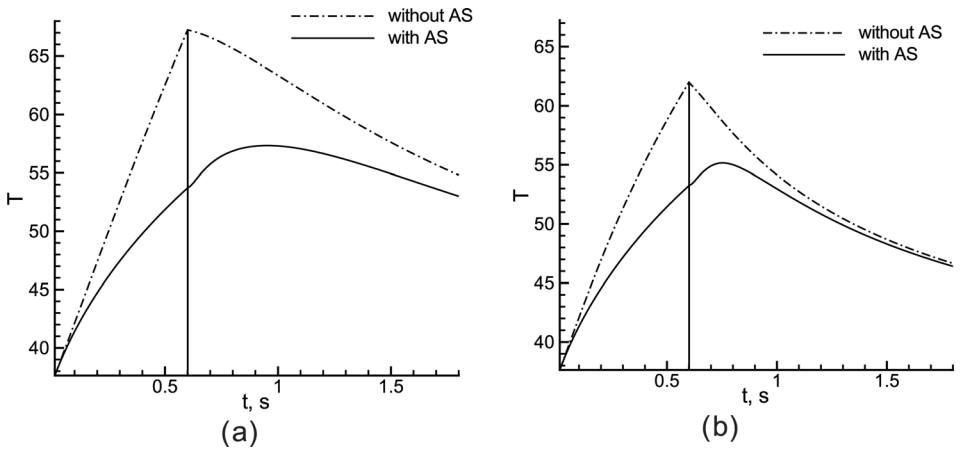

FIG. 10. The predicted temperatures on the blood vessel wall as a function of time for the sonication time 0.6 s (a) in the vein (velocity = 0.016 m/s); (b) in the artery (velocity = 0.13 m/s).

the tissue temperature proximal to the blood vessel is below the denaturation threshold.[12,16,22] For smaller sonication times the convective cooling effect in large blood vessels becomes less important. Figures 7(b) and 7(c) show that for an exposure time less than 2 s and for a focal pressure P_L larger than 6 MPa the tissue close to the blood vessel can be ablated. High focal intensity and small exposure time are two factors to ablate tumors proximal to large blood vessels. As it was shown in Sec. III B, a nonlinear propagation effect helps to ablate tumors close to large blood vessels. For different transducers' geometry nonlinear propagation effects start to play a role at different intensity levels. We are going to investigate whether nonlinear effects are necessary or just increasing the power deposition and neglecting nonlinearity will help to ablate a tumor close to the blood vessel wall. In Fig. 11 the predicted lesion shapes for three cases are presented. The first two cases are the simulation results for linear ($P_L = 8.5$ MPa) and nonlinear Westervelt equations for the same transducer parameters and peak power depositions $q_L = 364\ \mathrm{W/cm^3}$ and $q_{\mathrm{Nonlinear}} = 494\ \mathrm{W/cm^3}$ [see Fig. 6(c)]. The third case (linear-norm) presents the results for the higher value of acoustic power and peak power deposition $q = q_{\mathrm{Nonlinear}} = 494\ \mathrm{W/cm^3}$. Due to the thermal diffusion the difference between the predicted lesions for the linear (solid line) and nonlinear (dashed-dotted line) theories is very small. However, nonlinear simulation results at high intensities predict that "boiling" will appear much faster than those in the case of solving the linear Westervelt equation (Fig. 8). The medical doctors should be aware of boiling because it alters the treatment and can lead to disruption of the vessel wall. An increase of power deposition and neglecting nonlinearity (dashed line) shows that a tumor can be ablated in this case. However the lesion (dashed line) will be overestimated in this case.

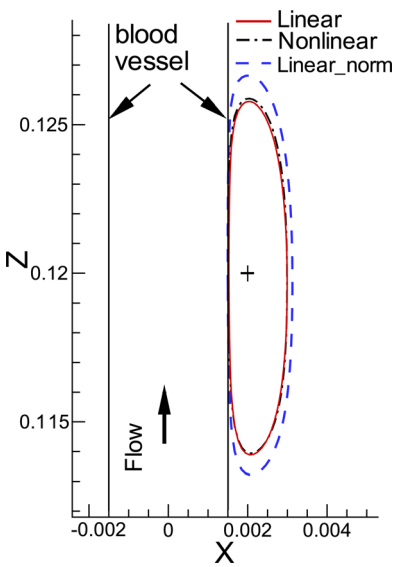

FIG. 11. (Color online) The predicted lesion shapes for three cases are presented. The first two cases are simulation results for linear ($P_L = 8.5$ MPa) and nonlinear Westervelt equations for the same transducer parameters and peak power depositions $q_L = 364\ \mathrm{W/cm^3}$ and $q_{\mathrm{Nonlinear}} = 494\ \mathrm{W/cm^3}$ [see Fig. 6(c)]. The third case (linear-norm) presents the results for the higher value of acoustic power for the linear Westervelt equation and peak power deposition $q = q_{\mathrm{Nonlinear}} = 494\ \mathrm{W/cm^3}$.

When the focal point is located inside the blood vessel, a large part of the energy will be carried away by the blood flow. Numerical simulation results show that in this case a layer of tissue close to the blood vessel wall will remain viable and recurrent cancer will appear. Therefore during focused ultrasound therapy the focal point should be located outside of the blood vessel.

IV. CONCLUSION

A physical model to conduct the current HIFU study is presented. The proposed model takes into account the convective cooling in a large blood vessel and the perfusion due to capillary flows. Convective cooling in a large blood vessel was shown to be able to reduce the temperature near a large blood vessel.[12,22,47] Acoustic streaming was also included in the simulation model. The effect of acoustic streaming was underestimated previously. In previous models, acoustic streaming velocity in a blood vessel during HIFU therapy was assumed to be less than the blood flow velocity[29] and was neglected.[30] In the present work it was first shown that the acoustic streaming velocity can be up to an order of magnitude larger than the velocity in a blood vessel. A focused ultrasound beam with the peak intensity $2470\ \mathrm{W/cm^2}$ can induce flow with the peak velocity up to 75 cm/s in a vessel with a diameter of 3 mm. The predicted temperature difference for the cases considered with and without acoustic streaming effect is 13.5 °C or 81% difference on the blood vessel wall for the vein. For a smaller diameter of a blood vessel the effects of blood flow cooling and acoustic streaming on the temperature distribution become smaller.[13] At high intensities cooling by acoustic streaming can prevail over convective cooling in a large blood vessel. This demonstrates the necessity of taking into account both the convective cooling and acoustic streaming effects for a simulation involving a large blood vessel, when the tumor is close to a large blood vessel. Owing to nonlinear effects the temperature in the focal region can be significantly increased in comparison with the linear case and can help to ablate the tumor close to the blood vessel. The theoretical feasibility to necrotize the tumors close to major hepatic arteries and veins was shown.

ACKNOWLEDGMENTS

The authors would like to acknowledge the financial support from the Center for Advanced Studies on Theoretical Science (CASTS) and from the National Science Council of Republic of China under Contract No. NSC102-2811-M-002-125.

[1]Y. F. Zhou, "High intensity focused ultrasound in clinical tumor ablation," World J. Clin. Oncol. **2**, 8–27 (2011).
[2]T. A. Leslie and J. E. Kennedy, "High intensity focused ultrasound in the treatment of abdominal and gynaecological diseases," Int. J. Hyperthermia **23**, 173–182 (2007).
[3]N. T. Wright and J. D. Humphrey, "Denaturation of collagen via heating: An irreversible rate process," Annu. Rev. Biomed. Eng. **4**, 109–128 (2002).
[4]S. A. Sapareto and W. C. Dewey, "Thermal dose determination in cancer therapy," Int. J. Radiat. Oncol. Biol. Phys. **10**(6), 787–800 (1984).

[5]J. S. Huang, D. A. Gervais, and P. R. Mueller, "Radiofrequency ablation: Review of mechanism, indications, technique, and results," Chin. J. Radiol. **26**, 119–134 (2001).
[6]L. Frich, P. K. Hol, S. Roy, T. Mala, B. Edwin, O. P. Clausen, and I. P. Gladhaug, "Experimental hepatic radiofrequency ablation using wet electrode: Electrode-to-vessel distance is a significant predictor for delayed portal vein thrombosis," Eur. Radiol. **16**, 1990–1999 (2006).
[7]T. W. H. Sheu, C. W. Chou, S. F. Tsai, and P. C. Liang, "Three-dimensional analysis for radiofrequency ablation of liver tumor with blood perfusion effect," Comput. Methods Biomech. Biomed. Eng. **8**(4), 229–240 (2005).
[8]L. Zhang, H. Zhu, C. Jin, K. Zhou, K. Li, H. Su, W. Chen, J. Bai, and Z. Wang, "High-intensity focused ultrasound (HIFU): Effective and safe therapy for hepatocellular carcinoma adjacent to major hepatic veins," Eur. Radiol. **19**, 437–445 (2009).
[9]H. H. Pennes, "Analysis of tissue and arterial blood temperature in the resting human forearm," J. Appl. Physiol. **1**, 93–122 (1948).
[10]P. M. Meaney, M. D. Cahill, and G. R. ter Haar, "The intensity dependence of lesion position shift during focused ultrasound surgery," Ultrasound Med. Biol. **26**(3), 441–450 (2000).
[11]M. S. Canney, V. A. Khokhlova, O. V. Bessonova, M. R. Bailey, and L. A. Crum, "Shock-induced heating and millisecond boiling in gels and tissue due to high intensity focused ultrasound," Ultrasound Med. Biol. **36**, 250–267 (2010).
[12]M. C. Kolios, M. D. Sherar, and J. W. Hunt, "Large blood vessel cooling in heated tissues: A numerical study," Phys. Med. Biol. **40**, 477–494 (1995).
[13]M. A. Solovchuk, T. W. H. Sheu, M. Thiriet, and W. L. Lin, "On a computational study for investigating acoustic streaming and heating during focused ultrasound ablation of liver tumor," Appl. Ther. Eng. **56**(1–2), 62–76 (2013).
[14]F. P. Curra, P. D. Mourad, V. A. Khokhlova, R. O. Cleveland, and L. A. Crum, "Numerical simulations of heating patterns and tissue temperature response due to high-intensity focused ultrasound," IEEE Trans. Ultrason. Ferroelectr. Freq. Control **47**, 1077–1089 (2000).
[15]T. W. H. Sheu, M. A. Solovchuk, A. W. J. Chen, and M. Thiriet, "On an acoustics-thermal-fluid coupling model for the prediction of temperature elevation in liver tumor," Int. J. Heat Mass Transfer **54**(17–18), 4117–4126 (2011).
[16]M. A. Solovchuk, T. W. H. Sheu, W. L. Lin, I. Kuo, and M. Thiriet, "Simulation study on acoustic streaming and convective cooling in blood vessels during a high-intensity focused ultrasound thermal ablation," Int. J. Heat Mass Transfer **55**(4), 1261–1270 (2012).
[17]J. N. Tjotta, S. Tjotta, and E. H. Vefring, "Effects of focusing on the nonlinear interaction between two collinear finite amplitude sound beams," J. Acoust. Soc. Am. **89**, 1017–1027 (1991).
[18]J. E. Soneson, "A parametric study of error in the parabolic approximation of focused axisymmetric ultrasound beams," J. Acoust. Soc. Am. **131**, EL481–EL485 (2012)
[19]M. S. Canney, M. R. Bailey, L. A. Crum, V. A. Khokhlova, and O. A. Sapozhnikov, "Acoustic characterization of high intensity focused ultrasound fields: A combined measurement and modeling approach," J. Acoust. Soc. Am. **124**, 2406–2420 (2008).
[20]J. Tavakkoli, D. Cathignol, R. Souchon, and O. A. Sapozhnikov, "Modeling of pulsed finite-amplitude focused sound beams in time domain," J. Acoust. Soc. Am. **104**, 2061–2072 (1998).
[21]P. V. Yuldashev and V. A. Khokhlova, "Simulation of three-dimensional nonlinear fields of ultrasound therapeutic arrays," Acoust. Phys. **57**(3), 334–343 (2011).
[22]P. Hariharan, M. R. Myers, and R. K. Banerjee, "HIFU procedures at moderate intensities—effect of large blood vessels," Phys. Med. Biol. **52**(12), 3493–3513 (2007).
[23]M. A. Solovchuk, T. W. H. Sheu, and M. Thiriet, "Effects of acoustic nonlinearity and blood flow cooling during HIFU treatment," AIP Conf. Proc. **1503**, 83–88 (2012).
[24]K. R. Nightingale, P. J. Kornguth, W. F. Walker, B. A. McDermott, and G. E. Trahey, "A novel ultrasonic technique for differentiating cysts from solid lesions: Preliminary results in the breast," Ultrasound Med. Biol. **21**, 745–751 (1995).
[25]F. A. Duck, "Radiation pressure and acoustic streaming," in *Ultrasound in Medicine*, edited by F. A. Duck, A. C. Baker, and H. C. Starritt (Institute of Physics Publishing, Bristol, 1998), Chap. 3.
[26]C. Eckart, "Vortices and streams caused by sound waves," Phys. Rev. **73**, 68–76 (1948).
[27]W. L. Nyborg, "Acoustic streaming," in *Nonlinear Acoustics*, edited by M. F. Hamilton and D. T. Blackstock (Academic Press, San Diego, 1998), Chap. 7.
[28]X. Shi, R. W. Martin, S. Vaezy, and L. A. Crum, "Quantitative investigation of acoustic streaming in blood," J. Acoust. Soc. Am. **111**(2), 1110–1121 (2002).
[29]C. C. Coussios and R. A. Roy, "Applications of acoustics and cavitation to non-invasive therapy and drug delivery," Annu. Rev. Fluid Mech. **40**, 395–420 (2008).
[30]M. Bailey, V. Khokhlova, O. Sapozhnikov, S. Kargl, and L. Crum, "Physical mechanism of the therapeutic effect of ultrasound (A review)," Acoust. Phys. **49**(4), 369–388 (2003).
[31]M. A. Solovchuk, T. W. H. Sheu, and M. Thiriet, "The effects of acoustic streaming on the temperature distribution during focused ultrasound therapy," AIP Conf. Proc. **1433**, 589–592 (2012).
[32]M. F. Hamilton and D. T. Blackstock, *Nonlinear Acoustics* (Academic Press, San Diego, 1998), 455 pp.
[33]Y. Jing and R. O. Cleveland, "Modeling the propagation of nonlinear three-dimensional acoustics beams in inhomogeneous media" J. Acoust. Soc. Am. **122**(3), 1352–1364 (2007).
[34]A. D. Pierce, *Acoustics, an Introduction to its Physical Principles and Applications* (Acoustical Society of America, New York, 1991), 678 pp.
[35]X. Yang and R. O. Cleveland, "Time domain simulation of nonlinear acoustic beams generated by rectangular pistons with application to harmonic imaging," J. Acoust. Soc. Am. **117**(1), 113–123 (2005).
[36]Q.-H. Liu and J. Tao, "The perfectly matched layer for acoustic waves in absorptive media," J. Acoust. Soc. Am. **102**, 2072–2082 (1997).
[37]I. Hallaj and R. Cleveland, "FDTD simulation of finite-amplitude pressure and temperature fields for biomedical ultrasound," J. Acoust. Soc. Am. **105**(5), L7–L12 (1999).
[38]T. Kamakura, M. Matsuda, Y. Kumamoto, and M. A. Breazeale, "Acoustic streaming induced in focused Gaussian beams," J. Acoust. Soc. Am. **97**, 2740–2746 (1995).
[39]H. T. O'Neil, "Theory of focusing radiators," J. Acoust. Soc. Am. **21**(5), 516–526 (1949).
[40]T. W. H. Sheu, C. F. Chen, and L. W. Hsieh, "Development of a three-point sixth-order compact Helmholtz scheme for scattering wave propagation," J. Comput. Acoust. **16**(3), 343–359 (2008).
[41]D. T. Blackstock, "Connection between the Fay and Fubini solutions for plane sound waves of finite amplitude," J. Acoust. Soc. Am. **14**, 1019–1026 (1965).
[42]O. Bessonova and V. Wilkens, "Membrane hydrophone measurement and numerical simulation of HIFU fields up to developed shock regimes," IEEE Trans. Ultrason. Ferroelectr. Freq. Control **60**(2), 290–299 (2013).
[43]F. A. Duck, *Physical Property of Tissues—A Comprehensive Reference Book* (Academic Press, London, 1990), 346 pp.
[44]S. F. Tsai, T. W. H. Sheu, and T. M. Chang, "Lung effect on the hemodynamics in pulmonary artery," Int. J. Numer. Methods Fluids, **36**, 249–263 (2001).
[45]T. W. H. Sheu, S. K. Wang, and S. F. Tsai, "Finite element analysis of particle motion in steady inspiratory airflow," Comput. Methods Appl. Mech. Eng. **191**(25–26), 2681–2698 (2002).
[46]T. W. H. Sheu, S. F. Tsai, and I. S. Chiu, "A computational assessment of two arterial switch operations," Int. J. Comput. Fluid Dyn. **30**(3–4), 183–192 (2006).
[47]J. Huang, R. G. Holt, R. O. Cleveland, and R. A. Roy, "Experimental validation of a tractable medical model for focused ultrasound heating in flow-through tissue phantoms," J. Acoust. Soc. Am. **116**(4), 2451–2458 (2004).
[48]E. A. Filonenko and V. A. Khokhlova, "Effect of acoustic nonlinearity on heating of biological tissue by high-intensity focused ultrasound," Acoust. Phys. **47**(4), 468–475 (2001).
[49]T. D. Khokhlova, M. S. Canney, V. A. Khokhlova, O. A. Sapozhnikov, L. A. Crum, and M. R. Bailey, "Controlled tissue-emulsification produced by high intensity focused ultrasound shock waves and millisecond boiling," J. Acoust. Soc. Am. **130**, 3498–3510 (2011).
[50]W. S. Chen, C. Lafon, T. J. Matula, S. Vaezy, and L. A. Crum, "Mechanisms of lesion formation in high intensity focused ultrasound therapy," ARLO **4**(2), 41–46 (2003).
[51]V. A. Khokhlova, M. R. Bailey, J. A. Reed, B. W. Cunitz, P. J. Kaczkowski, and L. A. Crum, "Effects of nonlinear propagation, cavitation and boiling in lesion formation by high intensity focused ultrasound in a gel phantom," J. Acoust. Soc. Am. **119**(3), 1834–1848 (2006).

[52]S. Vaezy, R. Martin, and L. Crum, "High intensity focused ultrasound: A method of hemostasis," Echocardiogr. **18**(4), 309–315 (2001).
[53]J. A. Sherman and H. T. Davies, "Ultracision: The harmonic scalpel and its possible uses in maxillofacial surgery," Br. J. Oral Maxillofac Surg. **38**(5), 530–532 (2000).
[54]E. Bell, "The action of ultrasound on the mouse liver," J. Cell Comp. Physiol. **50**, 83–103 (1957).
[55]M. Dyson, J. B. Pond, B. Woodward, and J. Broadbent, "The production of blood cell stasis and endothelial damage in the blood vessels of chick embryos treated with ultrasound in a stationary wave field," Ultrasound Med. Biol. **1**, 133–148 (1974).
[56]G. R. ter Haar, M. Dyson, and S. P. Smith, "Ultrastructural changes in the mouse uterus brought about by ultrasonic irradiation at therapeutic intensities in standing wave fields," Ultrasound Med. Biol. **5**, 167–179 (1979).
[57]G. R. ter Haar, "Ultrasonic biophysics," in *Physical Principles of Medical Ultrasonics*, edited by C. R. Hill, J. C. Bamber, and G. R. ter Haar (John Wiley & Sons, Chichester, 2004), Chap. 12, pp. 349–407.